

# Simulation of Ion Dynamics in a Linear Paul Trap

Mark Kokish  
e-mail: mkokish@berkeley.edu

May 17, 2013

## 1 Theory

The potential in a Paul trap can be represented as a sum of static and dynamic terms. Following Leibfried, et al. [1], the potential is given by:

$$\Phi(x, y, z, t) = U \frac{1}{2} (\alpha x^2 + \beta y^2 + \gamma z^2) + \tilde{U} \cos(\omega_{rf} t) \frac{1}{2} (\alpha' x^2 + \beta' y^2 + \gamma' z^2) \quad (1)$$

where  $\omega_{rf}$  is the angular trap frequency. The geometric constraints:

$$-(\alpha + \beta) = \gamma > 0 \quad (2)$$

$$\alpha' = -\beta' \quad (3)$$

satisfy the Laplace equation  $\nabla \Phi = 0$  while enforcing static confinement in the z direction and dynamic confinement in the x-y plane. In the x direction, the classical equation of motion is given by:

$$\ddot{x} = -\frac{Z|e|}{m} \frac{\delta \Phi}{\delta x} [U\alpha + \tilde{U} \cos(\omega_{rf} t) \alpha'] x \quad (4)$$

Using the substitutions:

$$\xi = \frac{\omega_{rf} t}{2} \quad a_x = \frac{4Z|e|U\alpha}{m\omega_{rf}^2} \quad q_x = \frac{2Z|e|\tilde{U}\alpha'}{m\omega_{rf}^2} \quad (5)$$

Equation 4 can be transformed into the standard form of the Mathieu equation:

$$\frac{\delta^2 x}{\delta \xi^2} + [a_x - 2q_x \cos(2\xi)] x = 0 \quad (6)$$

Following the derivation presented in Leibfried, et al., ion motion in the x direction to the lowest order approximation ( $|a_x|, q_x^2 \ll 1$ ), is given by:

$$x(t) \approx 2AC_0 \cos\left(\beta_x \frac{\omega_{rf}}{2} t\right) \left[1 - \frac{a_x}{2} \cos(\omega_{rf} t)\right] \quad (7)$$

where

$$\beta_x \approx \sqrt{a_x + q_x^2/2} \quad (8)$$

and  $a_x$  and  $q_x$  are given by Equation 5.

Using the experimental parameters defined in Zhang, et al [2]:

$$U = \frac{\kappa V_{ec}}{z_0^2} \quad \tilde{U} = \frac{4V_0}{r_0^2} \quad \alpha = 1 \quad \beta = \alpha' = \beta' = -1 \quad \gamma = 0 \quad \gamma' = 2 \quad (9)$$

which transforms Equation 1 into:

$$\Phi(x, y, z, t) = \frac{\kappa V_{ec}}{2z_0^2} (2z^2 - x^2 - y^2) + \frac{2V_0}{r_0^2} (x^2 - y^2) \cos(\omega_{rf} t) \quad (10)$$

for an ion near the trap center, where  $\kappa$  is a constant determined by the geometry of the trap,  $V_{ec}$  and  $V_0$  are the axial and radial trap voltages, respectively, and the radial and axial trap dimensions are given by  $r_0$  and  $z_0$ , respectively.

The axial angular trap frequency is determined by simple harmonic motion:

$$\omega_z = \sqrt{\frac{k}{m}} = \sqrt{\frac{|e|}{m} \frac{2\kappa V_{ec}}{z_0^2}} \quad (11)$$

The radial angular trap frequency is given by Equations 7 and 8:

$$\omega_x = \beta_x \frac{\omega_{rf}}{2} = \frac{1}{mr_0^2 z_0 \omega_{rf}} \sqrt{Z|e|(8Z|e|V_0^2 z_0^2) + \kappa m r_0^4 V_{ec} \omega_{rf}^2} \quad (12)$$

The secular motion of the ion is used to gauge its temperature, which is assumed to follow Boltzmann statistics:

$$\frac{2}{3k_b} E_{sec} = T_{sec} = \frac{1}{3Nk_b} m \sum_i^N (\langle \bar{v}_{ix}^2 \rangle + \langle \bar{v}_{iy}^2 \rangle + \langle \bar{v}_{iz}^2 \rangle) \quad (13)$$

where  $\bar{v}_{i\alpha} = (1/J) \sum_{j=1}^J v_{i\alpha}$  and  $J$  is the number of time steps per one rf period.  $\langle \dots \rangle$  denotes an average over many rf periods and  $N$  is the number of ions.

Doppler cooling of an atom is achieved by stimulating an electronic excitation using a red-detuned laser fixed in a particular spatial direction. The absorption event decreases the atom's momentum along the axis of the laser. Spontaneous emission gives the atom a recoil momentum in a random direction equal to the momentum lost during the absorption event. After many excitations, the momentum gained from spontaneous emission averages to zero due to its lack of net direction, whereas the loss of momentum from the absorption event is consistent to a particular direction. This is recognized as a net loss in the atom's momentum. The Doppler cooling limit is given by:

$$T_D = \frac{\hbar\gamma}{2k_b} \quad (14)$$

where  $\gamma$  is the natural linewidth of the electronic transition, i.e. the (natural lifetime) $^{-1}$ .

The rate of absorption/emission is assumed to be governed by the following equations:

$$\frac{dP_g}{dt} = -\Gamma_l P_g + \gamma P_e + \Gamma_l P_e \quad (15)$$

$$\frac{dP_e}{dt} = \Gamma_l P_g - \gamma P_e - \Gamma_l P_e \quad (16)$$

where  $\Gamma_l$  is the coupling between the laser and the transition, and  $P_g$  and  $P_e$  are the probabilities of the electron being in the ground and excited states, respectively. Note that:

$$P_g + P_e = 1 \quad (17)$$

Here we use the steady state approximation. i.e.:

$$\frac{dP_g}{dt} = \frac{dP_e}{dt} = 0 \quad (18)$$

Using Equation 17, one can solve for  $P_e$ :

$$P_e = \frac{\Gamma_l}{2\Gamma_l + \gamma} \quad (19)$$

In the steady state approximation,  $P_e$  is given by:

$$P_e = \frac{1}{2} \frac{s}{s+1} \quad (20)$$

where  $s$  is the saturation parameter. Using Equations 19 and 20, one can solve for  $s$ :

$$s = \frac{2\Gamma_l}{\gamma} \quad (21)$$

The generalized s is defined by:

$$s = \frac{\frac{\Omega^2}{2}}{\delta_{eff} + \frac{\gamma^2}{4}} \quad (22)$$

where  $\Omega$  is the Rabi frequency and  $\delta_{eff} = \Delta - \mathbf{k} \cdot \mathbf{v}$ ,  $\Delta$  is the detuning,  $\mathbf{k}$  is the normalized vector of the cooling laser, and  $\mathbf{v}$  is the normalized velocity vector of the particle [3].

For our system, we allow ourselves to set an arbitrary saturation,  $s_{beam}$ , for which the detuning is set to zero.

$$s_{beam} = \frac{\frac{\Omega^2}{2}}{\frac{\gamma^2}{4}} = \frac{2\Omega^2}{\gamma^2} \quad (23)$$

Using Equations 23 and 24, we can solve for s in terms of  $s_{beam}$ :

$$s = \frac{s_{beam}}{\left(\frac{2\delta_{eff}}{\gamma}\right)^2 + 1} \quad (24)$$

Now with Equations 21 and 24, we can express  $\Gamma_l$  in terms of experimental parameters:

$$\Gamma_l = \frac{\gamma}{2} \frac{s_{beam}}{\left(\frac{2\delta_{eff}}{\gamma}\right)^2 + 1} \quad (25)$$

Given all of the experimental parameters, we can define the probabilities of absorption and spontaneous/stimulated emission. For a given time step, dt, the probability of absorption is given by:

$$P_{abs} = \Gamma_l dt \quad (26)$$

The probability of emission is given by:

$$P_{emit} = (\gamma + \Gamma_l)dt \quad (27)$$

On each time step, a random number between 0 and 1 is generated. If the number is lower than  $P_{abs}$ , the ion will absorb a photon. While the ion is in the excited state, it cannot absorb another photon. Subsequently, another random number is generated and if its value is lower than  $P_{emit}$ , then the ion will emit a photon. In order to distinguish between stimulated and spontaneous emission, the random number is then compared against the probability of spontaneous emission:

$$P_{spont} = \gamma dt \quad (28)$$

If the number is lower than  $P_{spont}$ , the photon will emit in a random direction. If the number is between  $P_{spont}$  and  $P_{emit}$ , the photon will emit along the direction of the laser. The trajectories of the ions are computed using the velocity Verlet algorithm.

## 2 Conditions

### 2.1 Expected

The following values used for the simulation are summarized in Table 1:

Table 1: Simulation Parameters

Parameter	Value
$m$	$6.655 \times 10^{-26}$ kg
$Z$	1
$ e $	$1.602 \times 10^{-19}$ C
$\kappa$	0.5
$r_0$	0.0005 m
$z_0$	0.01 m
$\omega_{rf}$	$2\pi \times 30$ MHz
$\gamma$	$(7.1 \text{ ns})^{-1}$
$V_x$	41.9 V
$V_y$	45.6 V
$V_z$	16.4 V
$\mathbf{k}$	$\frac{2\pi}{396.847nm}(1, 1, 1)$
$\Delta$	-0.5

where the mass,  $m$  is that of a calcium atom and  $\gamma$  is the natural linewidth of the calcium  $3S_{\frac{1}{2}} \rightarrow 3P_{\frac{1}{2}}$ . The value of  $\Delta$  is set to provide optimal cooling and the  $\mathbf{k}$  indicates that the cooling beam addresses the all three directions equally, (i.e., the laser is oriented 45 degrees between each coordinate axis). Table 2 summarizes the trap frequencies and parameters expected for a single ion.

Table 2: Trap Parameters

Parameter	Value
$\omega_x$	$2\pi \times (0.95$ MHz)
$\omega_y$	$2\pi \times (1.05$ MHz)
$\omega_z$	$2\pi \times (0.1$ MHz)
$q_x$	$9.1 \times 10^{-2}$
$q_y$	$9.8 \times 10^{-2}$
$a_x$	$2.2 \times 10^{-5}$
$a_y$	$-2.2 \times 10^{-5}$

## 2.2 Measured

Figure 4 shows cooling from 1 Kelvin down to the Doppler Temperature. Figure 5 zooms in on the cooled state, an average of 1 indicates that the Doppler temperature has been reached.

The cooling laser is oriented such that all three spatial dimensions are addressed. The voltages in the x and y directions were chosen to be nondegenerate (95% and 105% of the desired trap frequency) in order to avoid continuous heating in the z direction.

Figure 7 shows cooling starting from 50 mK, the ion initially cools and then heats primarily along the z axis, causing the total energy to rise. This is due to the degeneracy.

The absolute position of a single ion was recorded, and a sine curve was fitted to the data. Motion in the x, y and z directions and their fits are represented in Figures 1, 2 and 3, respectively. Figure 6 shows a fit to the micromotion (zoomed in).

Table 3: Measured Trap Parameters

Parameter	Value
$\omega_x$	$2\pi \times (0.963$ MHz)
$\omega_y$	$2\pi \times (1.047$ MHz)
$\omega_z$	$2\pi \times (0.100$ MHz)
$\omega_{rf}$	$2\pi \times (29.989$ MHz)

## 3 Experiment

### 3.1 Overview

A linear chain of trapped calcium ions are cooled to the Doppler temperature, forming a Coulomb crystal. Blue-detuned light is then shined on the crystal in order to increase its temperature via Doppler heating. After enough time, the crystal undergoes a crystal-to-cloud phase transition, during which the temperature, fluorescence and rate of ion-swapping is monitored.

### 3.2 Finding the Melting Point

For a five ion crystal, it is difficult to determine the exact moment when a crystal becomes a cloud. Typically, the fluorescence rate of the ions can be used to estimate a phase transition, because the crystal typically undergoes a characteristic drop in fluorescence upon changing into a cloud. However, in some cases where much higher radial trap frequencies were used, the fluorescence also dropped rapidly without any ions swapping positions along the z-axis. In the cloud state, it is assumed that the ions will have all three translation degrees of freedom. For this reason, the rate of ions swapping along the z-axis serves as a better indicator for melting.

In order to estimate the melting point, the number of swaps was monitored during the course of heating for 100 traces. At 2000 swaps, the simulation was cut off. It is assumed that the crystal has melted when the swap rate becomes constant (the curve remains linear). A line is fit to the last 1000 points (the linear region) and the x-intercept is calculated. Over the 100 traces, a histogram of the x-intercepts is created, a Gaussian is fitted to it and its mean is taken as the melting point. A graph of this process is illustrated in Figure 8 and the histogram in Figure 9.

### 3.3 Using Fluorescence as a Measure of Crystal Phase

It is worth mentioning that the fluorescence rate for a crystal remains fairly constant; the fluorescence rate also remains fairly constant, yet it slightly decreases as the temperature of the cloud increases. Given that the transition between crystal and cloud is sudden and that the fluorescence level is fairly constant in both phases, one would expect to only measure two distinct fluorescence rates: high (crystal) and low (melted). For example, if one were to measure the fluorescence at the melting point 100 times and plot the result in a histogram, one would expect two distinct populations, melted and crystallized.

Based on movies ([link](#)) made of the melting process with 5 ions, it unclear where the exact melting point is. This is most likely because 5 ions is too small a crystal for a phase change to be obvious. This implies that there should be a single population of fluorescence measurements, rather than two, because the transition from crystal to cloud is not sudden. However, in previous experiments ([link the to writeup](#)), two distinct populations were unambiguously resolved. The reason for this was investigated in the simulation.

### 3.4 Finding the Correct Readout Detuning

Despite initially having only one population, it is possible that two distinct fluorescence populations can be measured when readout is performed using light that is detuned off resonance. This is due to the asymmetric shape of the fluorescence spectrum of an ion crystal. In order to demonstrate this effect, spectra were recorded for ion crystals at three different temperatures. The Gaussian fitted to the histogram in Figure 9 was used to determine the three times (temperatures) during the heating pulse: -2 sigma from the mean was taken to be the crystallized ("cooled") state, the mean was taken to be the melting ("middle") state, and 2 sigma from the mean was taken to be the melted ("melted") state. The three traces that had melting points closest to these specific times were used to create the spectra. The positions and velocities of each trace were used as initial conditions to take the spectra. The spectra were taken by letting ions evolve while exposed to different detunings of the laser for a specific readout time; different readout times were probed.

The results are presented in Figures 10 through 19. Several things are clear from the figures. One, the higher temperature crystals are clearly Doppler-broadened. Two, the lineshape becomes more asymmetrical as the readout time is increased. This is thought to be because the light affects the temperature

of the crystal during readout. The asymmetry is due to the fact that the red detuned light will cool the crystal (increasing its fluorescence), while the blue-detuned light heats the crystal (decreasing its fluorescence). Lastly, one can see that the peaks of the spectra for the higher temperature crystals are red-shifted. This is believed to be because the rate of laser cooling cannot immediately keep up with the rate of other heating processes that become more prevalent as the ions rise in temperature (i.e. RF heating).

Using this spectral information, one can pick a specific frequency to do readout that will asymmetrically affect the temperature of the crystal depending on its initial temperature. In Figure 23, the chosen frequency will be shifted red of the "cooled" ions, thereby cooling them more during readout, whereas this same frequency is shifted blue of the melting and melted ions, meaning the laser will cool the ions much slower or even heat the ions.

### 3.5 Results and Discussion

Using the chosen readout frequency, the experiment was performed. The ions were initially Doppler cooled for 1ms in order to bring them to the Doppler temperature. The ions were then heated slowly with blue-detuned light for a given time (determined previously). The readout light was then shined for 20ms while the fluorescence rate was recorded. The results are presented in Figure 24. The smaller space between the black bars indicates the regions where the total fluorescence was calculated and plotted in a histogram. These histograms are represented in Figures 25 through 28. Notice that initially, there is only one population of fluorescence measured. However, over time the population separates into a crystallized and melted population.

In order to probe the heating processes that might account for the spectral asymmetry, an experiment was done. The ions were heated for a certain amount of time, some of crystals would melt sooner than others (i.e. in some cases, the ions would already be cooled or melted by readout time). In each case, the total energy was monitored for a period of 20ms. The results are presented in Figure 21 (note that an experiment to make sure the total energy calculation was correct was done by using the pseudopotential and letting the ions evolve; the constant total energy in Figure 20 seems to indicate that the calculation is correct). Notice that RF-heating seems to only be present for the cases where the crystals have already started to melt (swap graph not included). In the cases where the crystal has already melted, the effect of RF heating is less prevalent, most likely due to the decreased interaction of the ions with each other. In either case, the RF heating seems to be minuscule compared to the efficiency of laser cooling. This means that most red-detuned light will eventually cool the crystal, as Figure 24 seems to imply (notice how at different times, different traces will spontaneously cool). However, this also means that RF-heating in this regime is likely not the main reason the peaks of the spectra shift red for the higher temperature crystals.

It was then speculated that perhaps a stray electric field would push the ions off-center, thereby increasing the micromotion of the ions, leading to stronger heating. An experiment was done to simulate the ions being pushed 5 microns off center by a constant electric field. As shown in Figure 22, the RF-heating did not increase dramatically. Therefore, it is likely that RF-heating is not the main process, which causes the shift.

In order to further probe the extent of heating, an experiment was done to see at which frequency of the laser would cooling match heating. Figures 29 through 31 indicate experiments where the initial conditions from the "cooled", "middle" and "melted" cases were used; the ions were then left to evolve under a specific frequency of light, the detuning of which is labelled for each curve. Note that in all cases, the on-resonance light heats the crystal. The frequencies are then scanned until a particular detuning is reached that seems to keep the total energy somewhat constant. It is worth noting that the detuning of the laser that balances the heating corresponds to the peak in the spectra taken for these cases (see Figure 16) except for the melted case. In the melted case, several detunings were tried that were near the peak for spectrum of the melted case (20 ms readout time); however, all detunings in this region rapidly cooled the crystal.

## References

- [1] Leibfried, D., et al. "Quantum dynamics of single trapped ions." *Reviews of Modern Physics* 75.1 (2003): 281.
- [2] Zhang, C. B., et al. "Molecular-dynamics simulations of cold single-species and multispecies ion ensembles in a linear Paul trap." *Physical Review A* 76.1 (2007): 012719.
- [3] Cohen-Tannoudji, Claude, et al. "Atom-Photon Interactions: Basic Processes and Applications." *Physics Today* 45 (1992): 115.

## A Supplementary Information

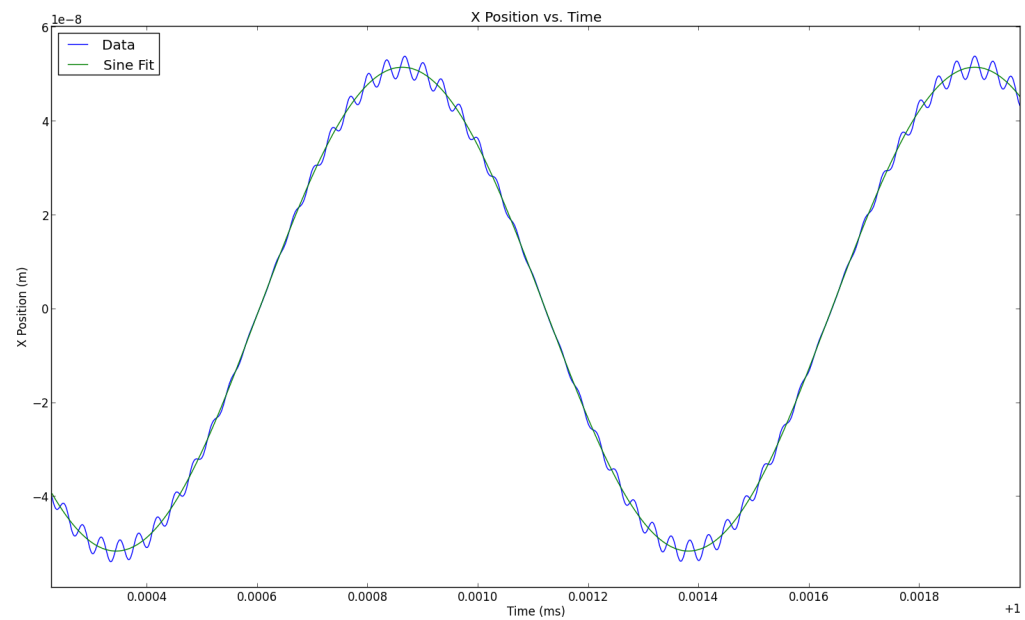


Figure 1: Single Ion Movement in the X Direction.

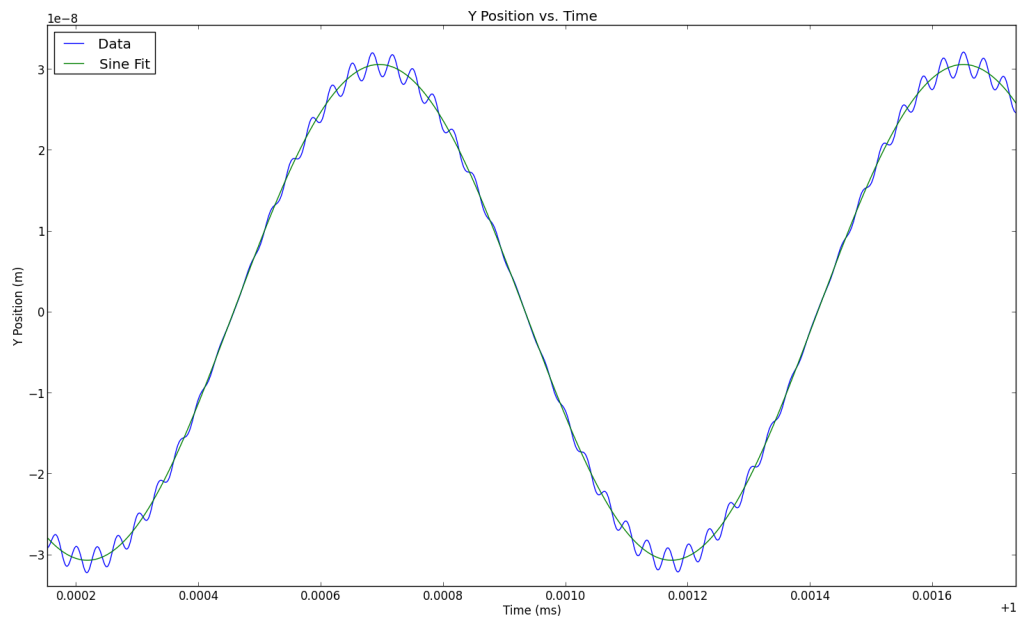


Figure 2: Single Ion Movement in the Y Direction.

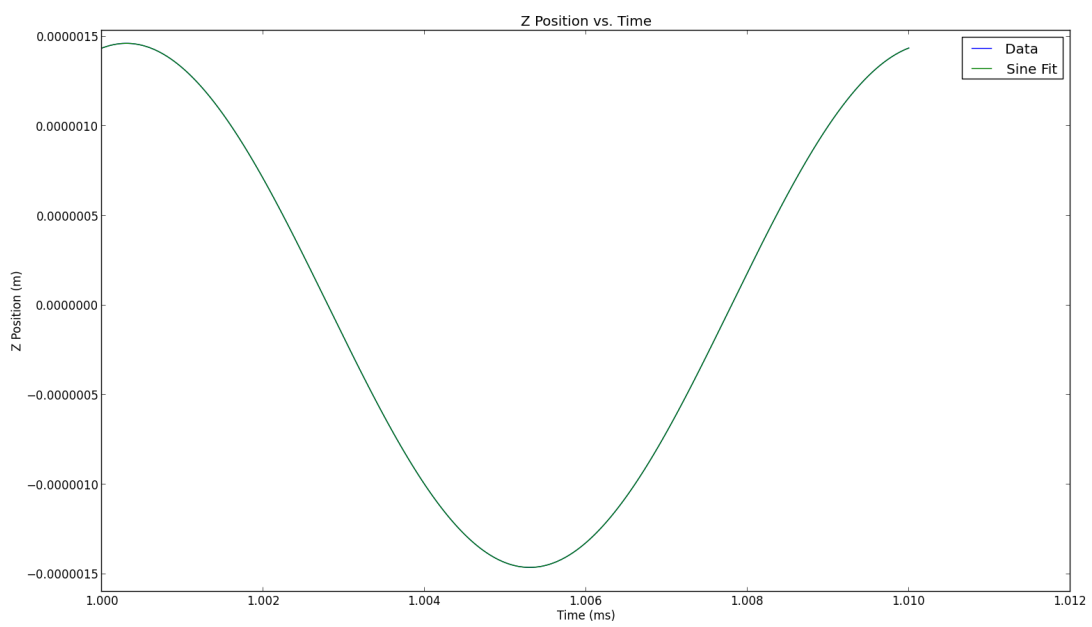


Figure 3: Single Ion Movement in the Z Direction.

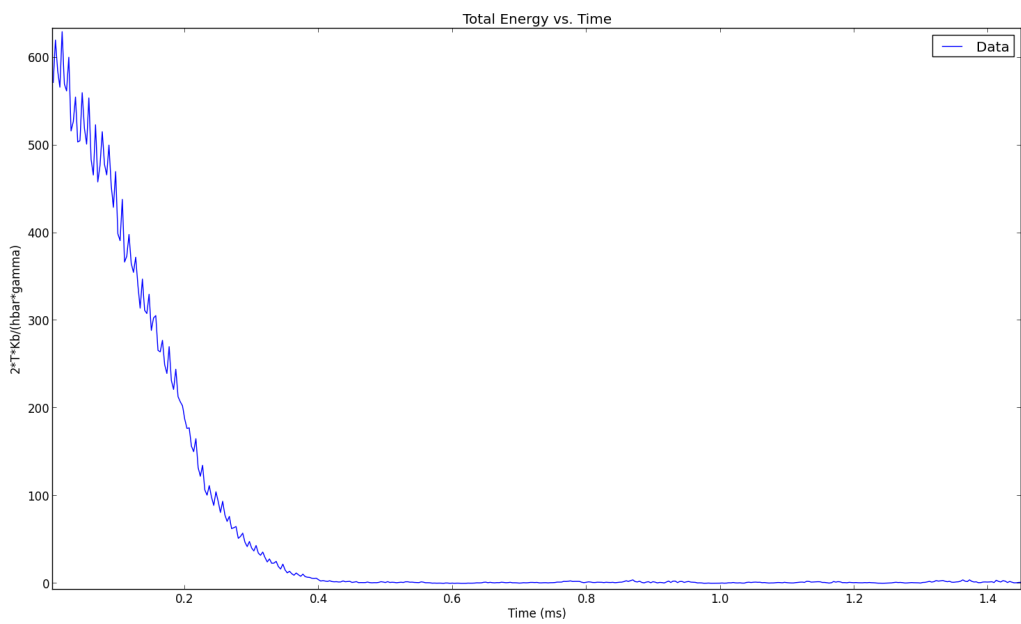


Figure 4: Doppler Cooling.

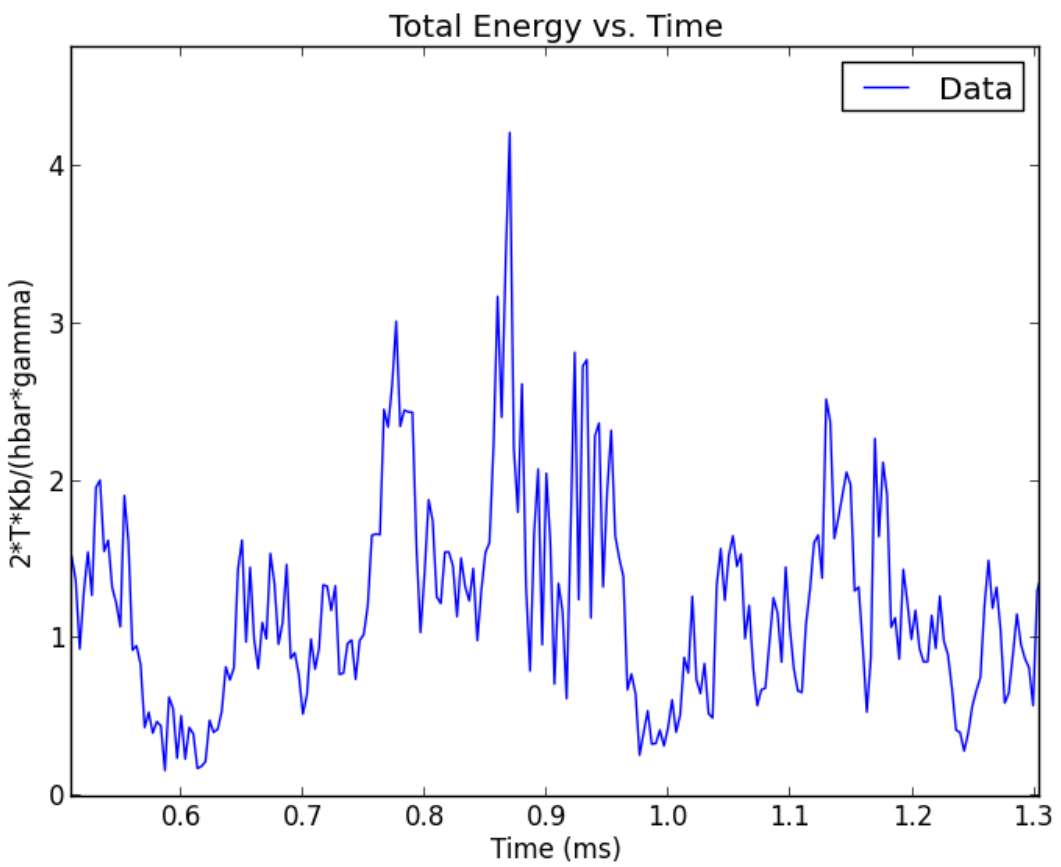


Figure 5: A Single Ion at the Doppler Temperature.

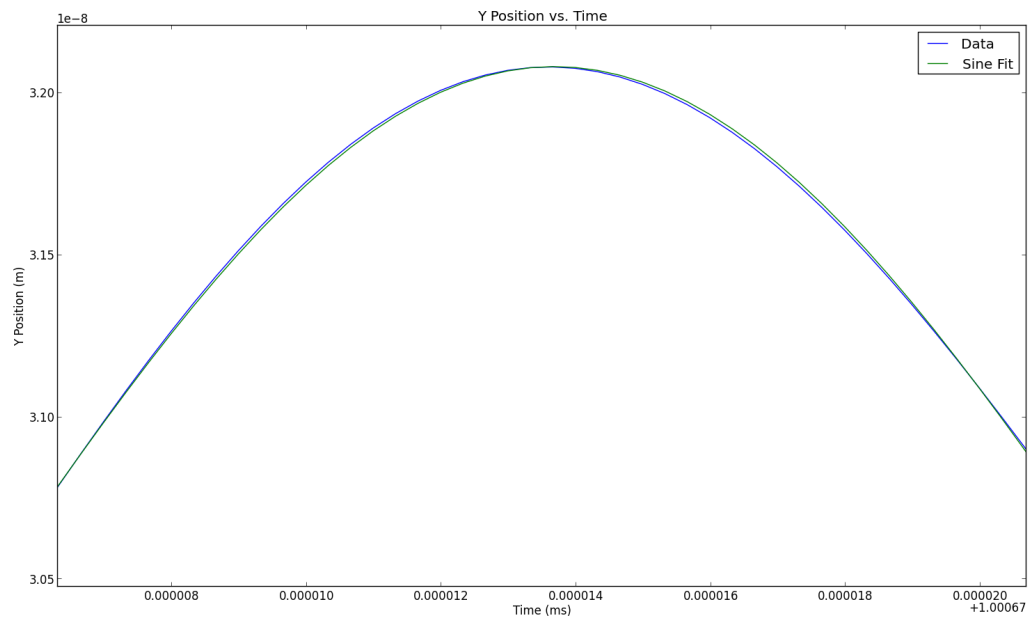


Figure 6: RF-Driven Peak (Micromotion).

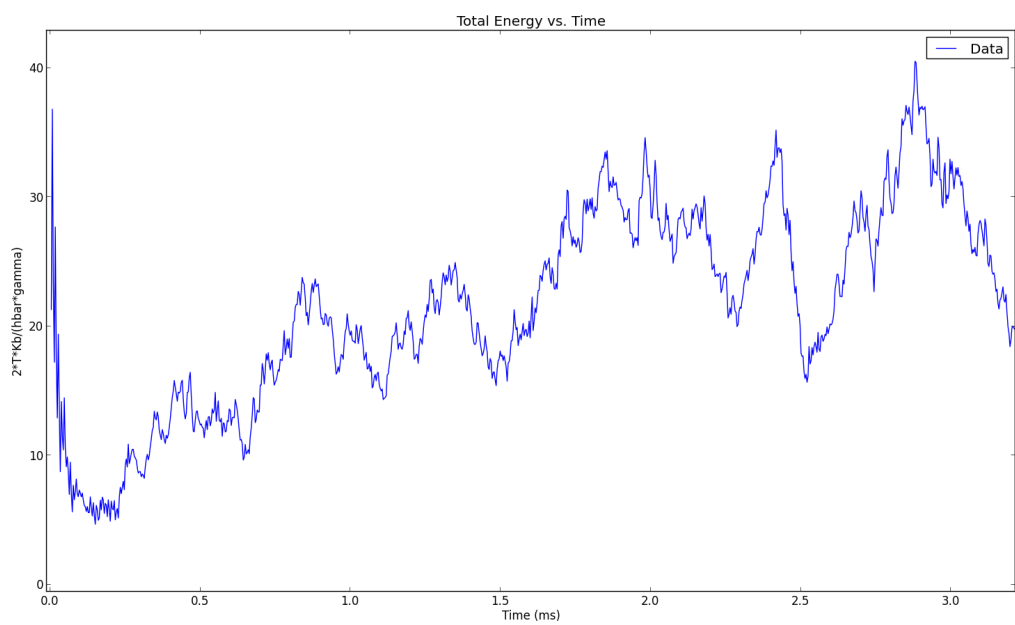


Figure 7: Degenerate Voltages in the Radial Direction Inhibits Cooling.

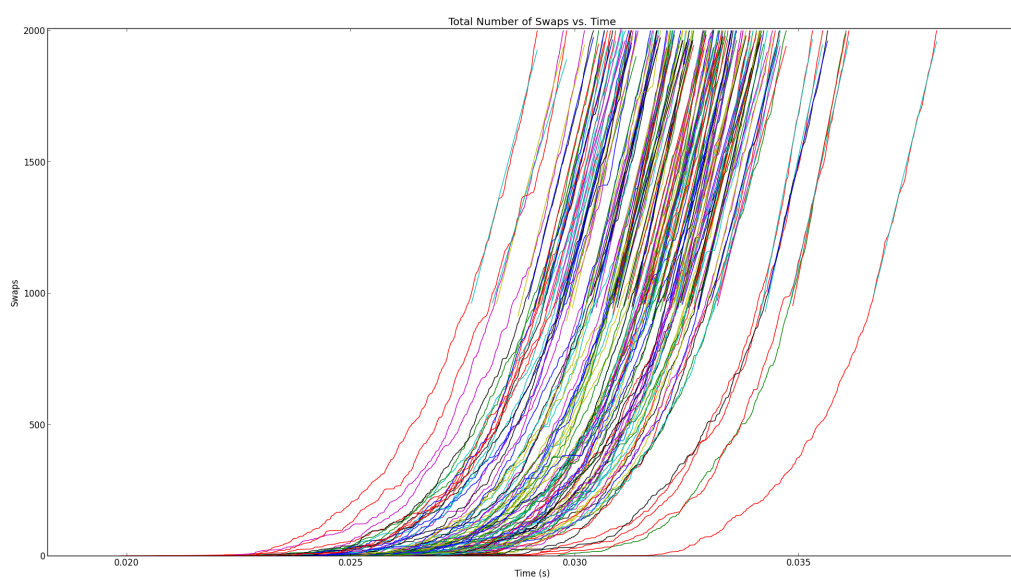


Figure 8: Swaps vs. Time for 100 Traces - Finding the Melting Point

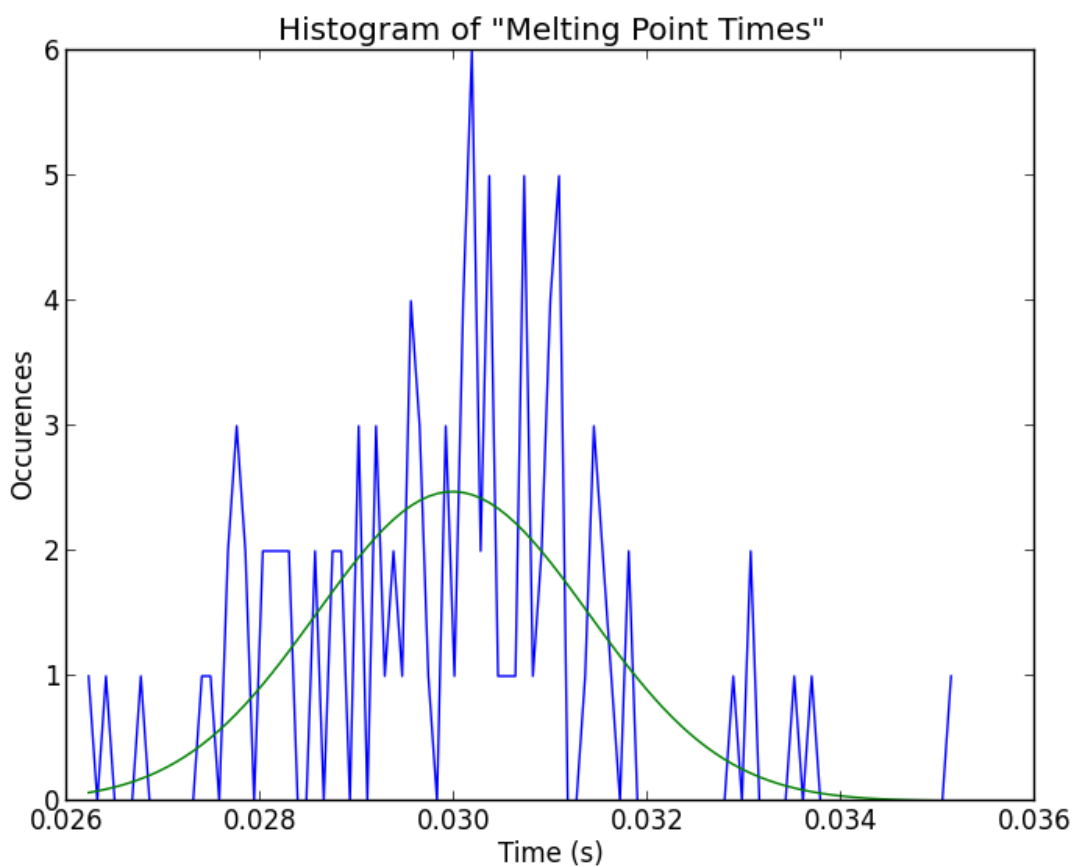


Figure 9: Histogram of X-intercepts - the mean indicates the melting point.

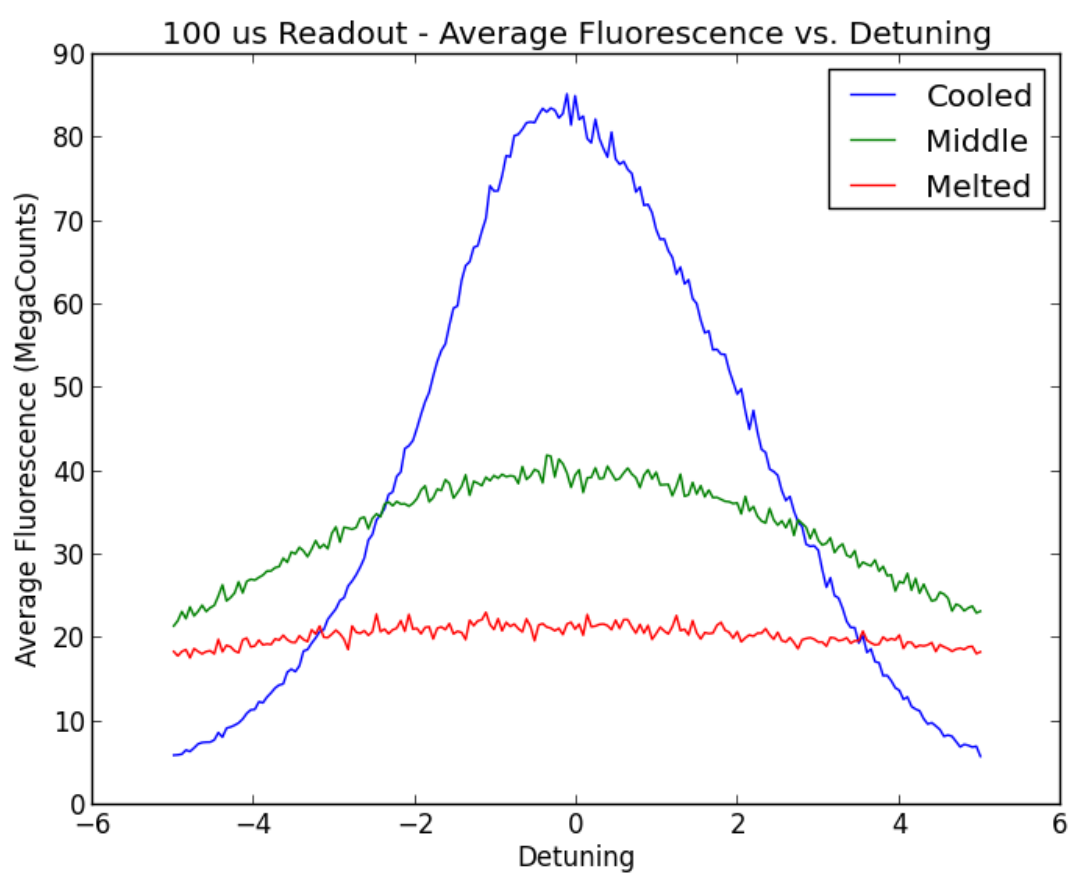


Figure 10: Spectra of crystals at three different temperatures with a readout time of 100  $\mu\text{s}$ .

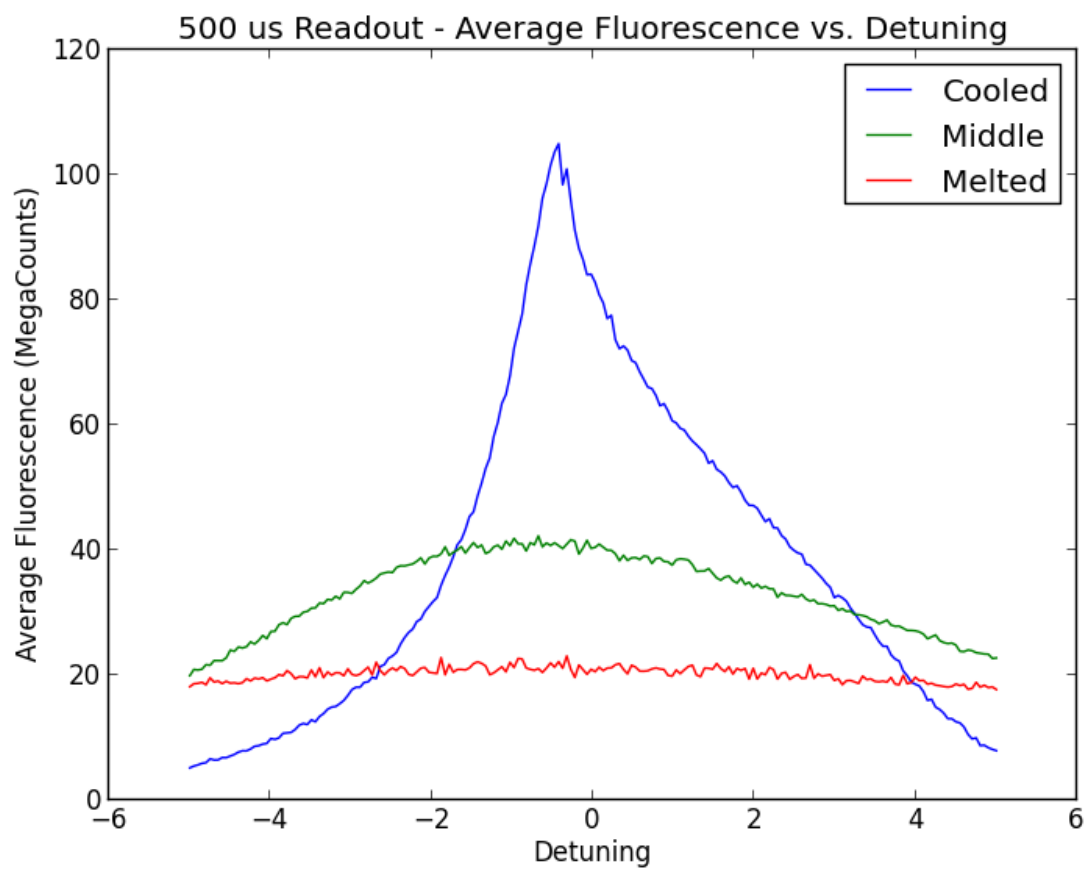


Figure 11: Spectra of crystals at three different temperatures with a readout time of 500  $\mu\text{s}$ .

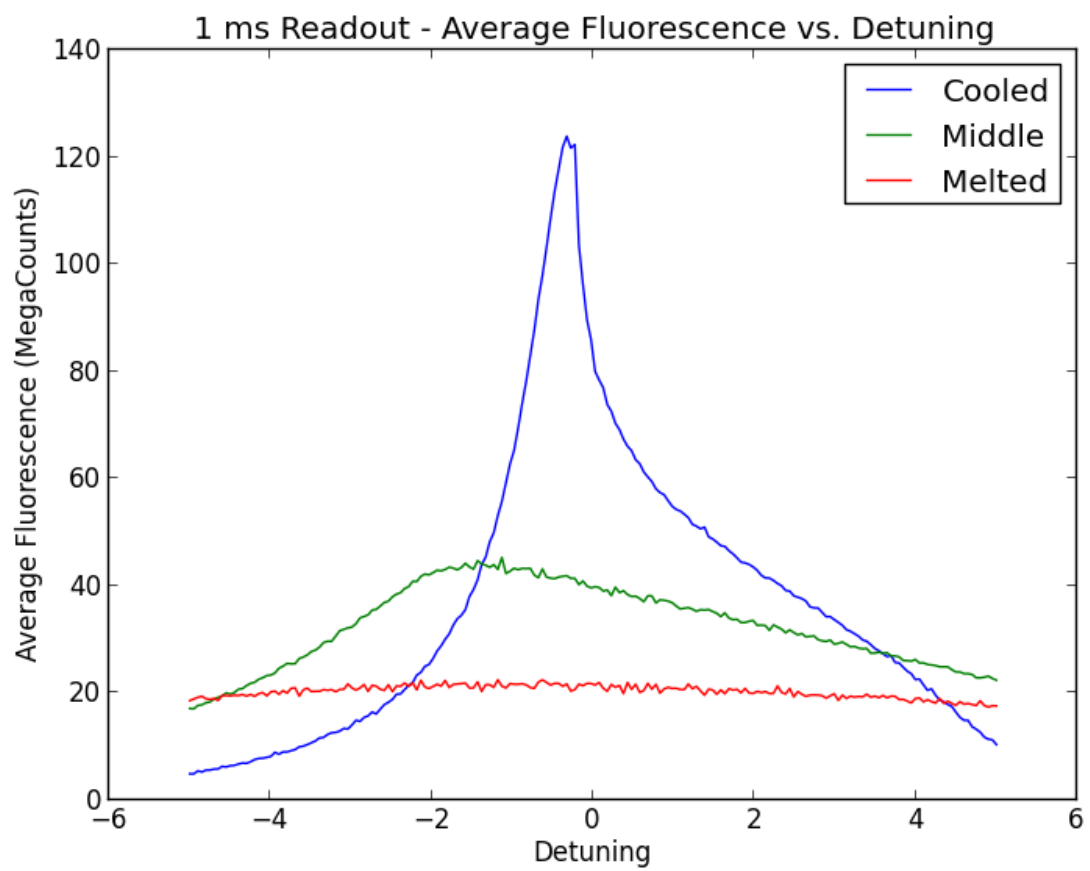


Figure 12: Spectra of crystals at three different temperatures with a readout time of 1 ms.

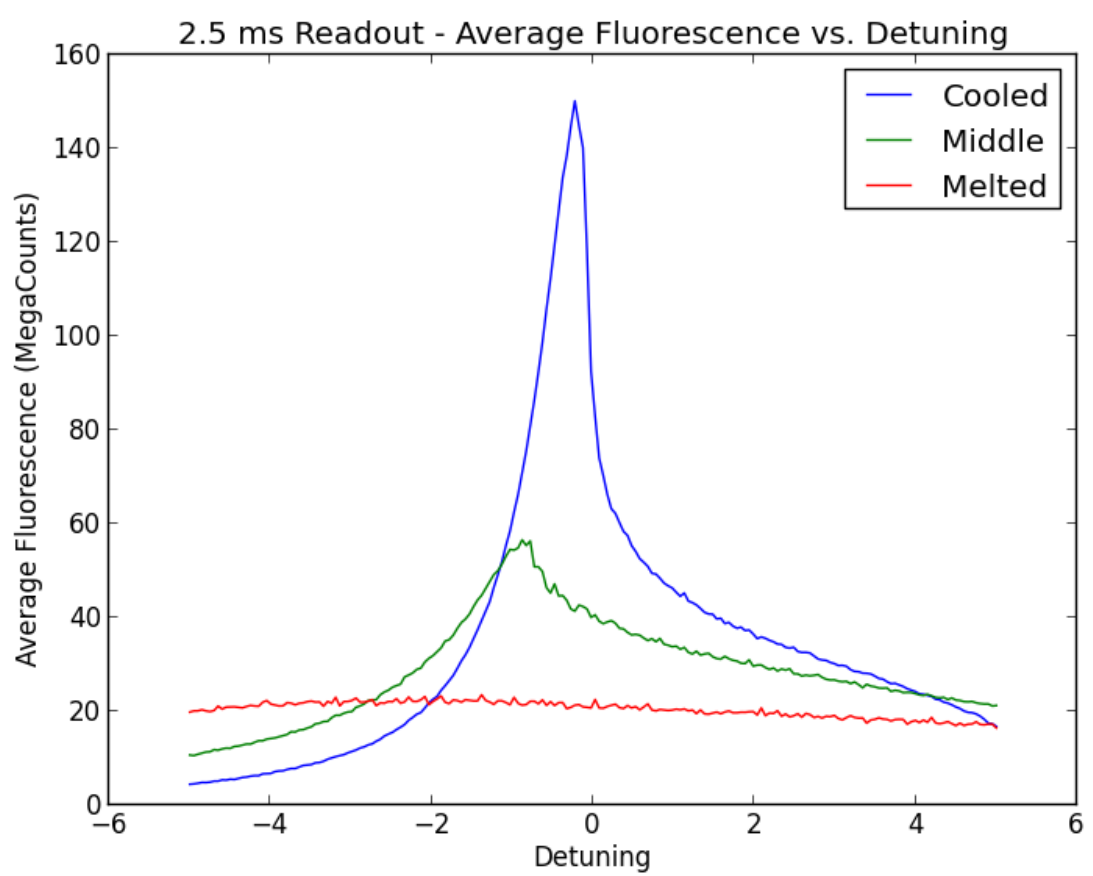


Figure 13: Spectra of crystals at three different temperatures with a readout time of 2.5 ms.

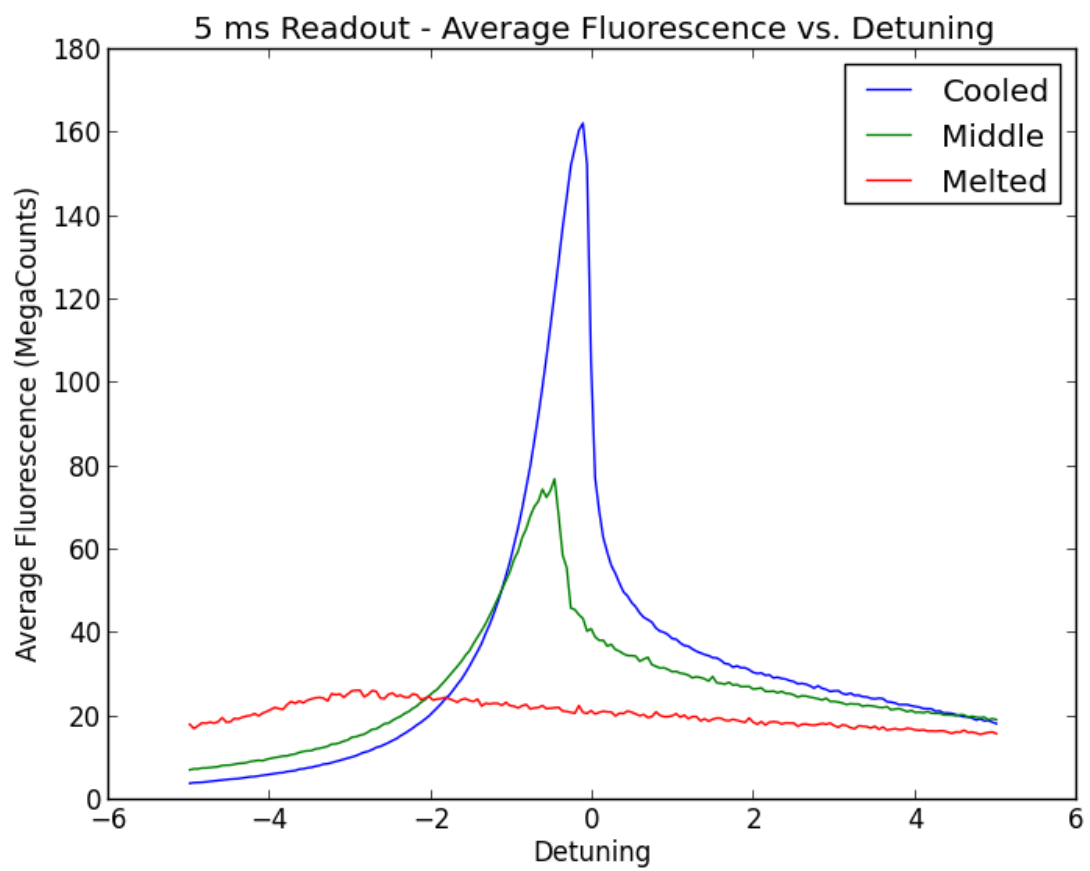


Figure 14: Spectra of crystals at three different temperatures with a readout time of 5 ms.

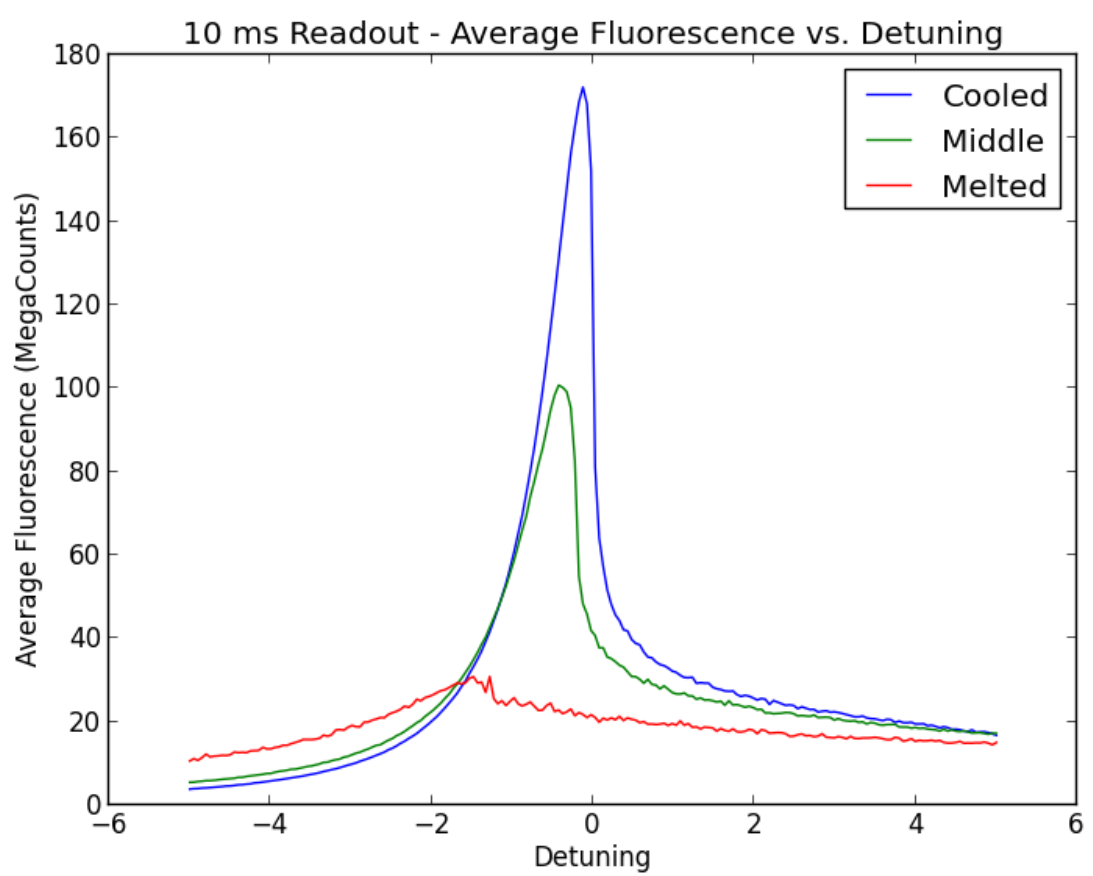


Figure 15: Spectra of crystals at three different temperatures with a readout time of 10 ms.

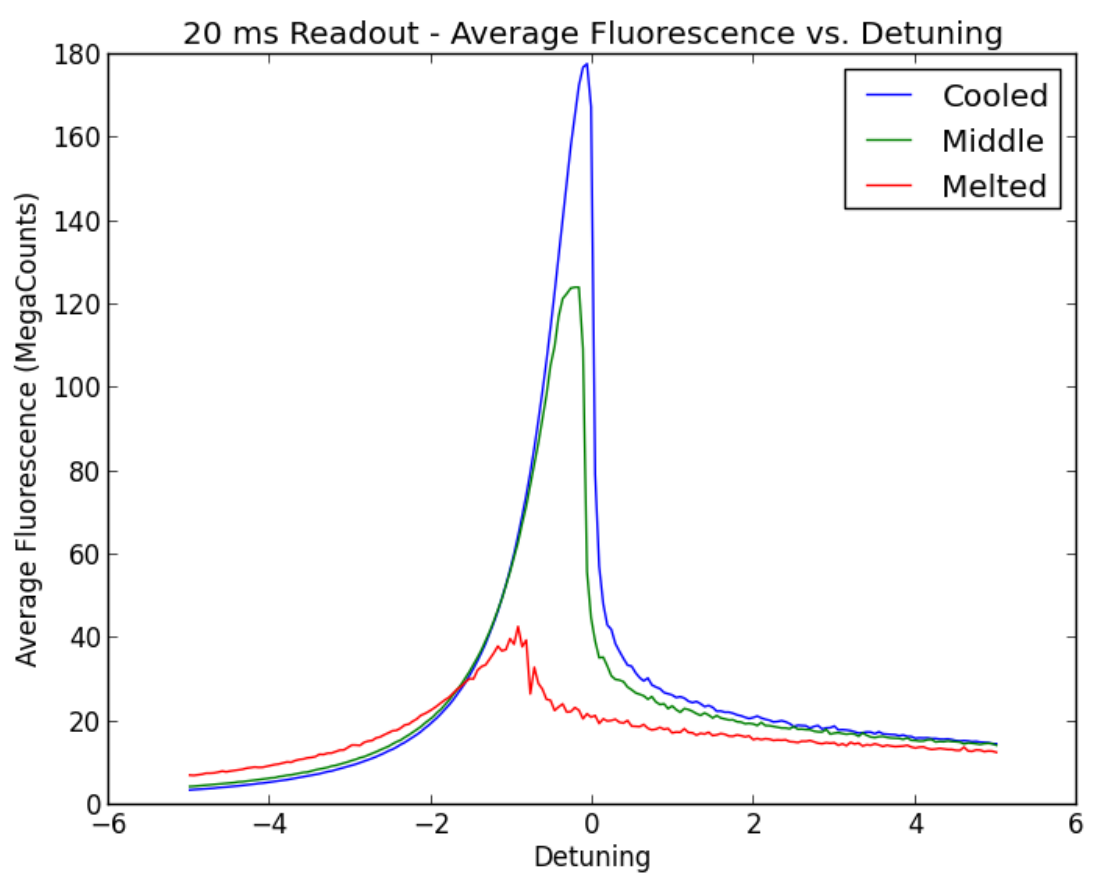


Figure 16: Spectra of crystals at three different temperatures with a readout time of 20 ms.

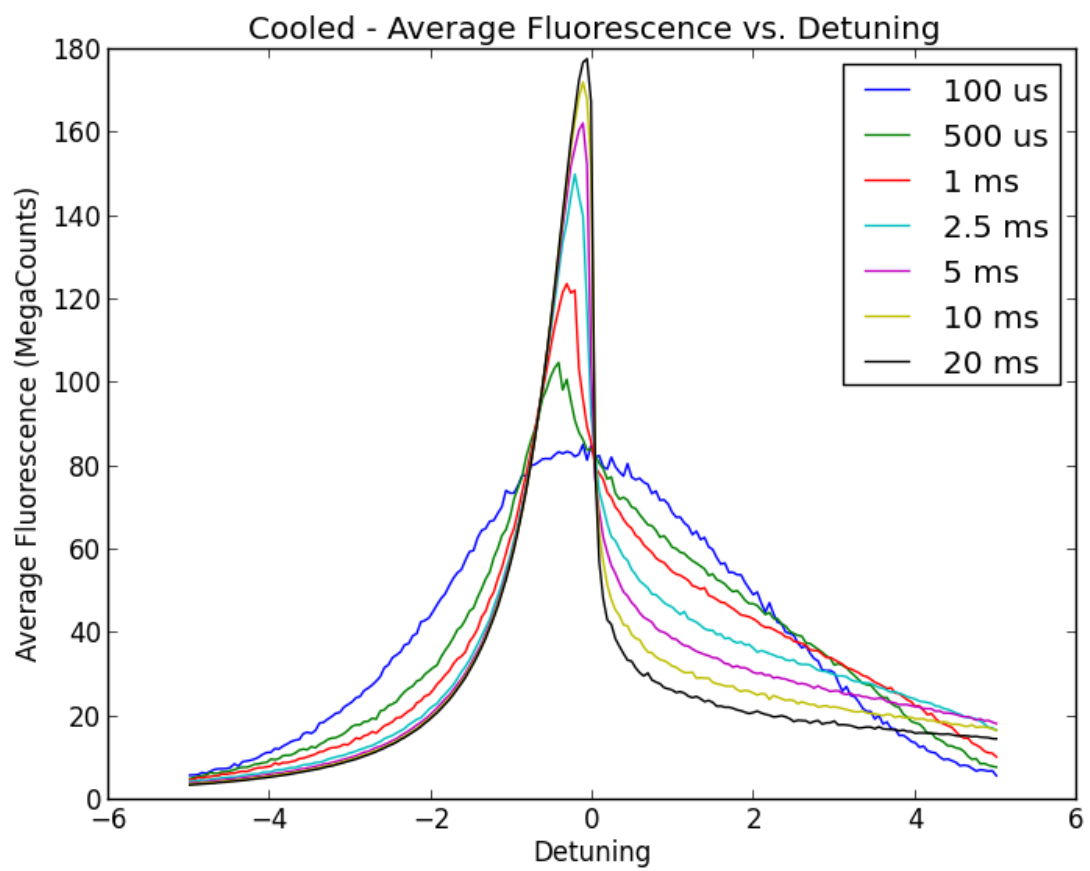


Figure 17: Spectra of the "cooled" crystal taken with different readout times.

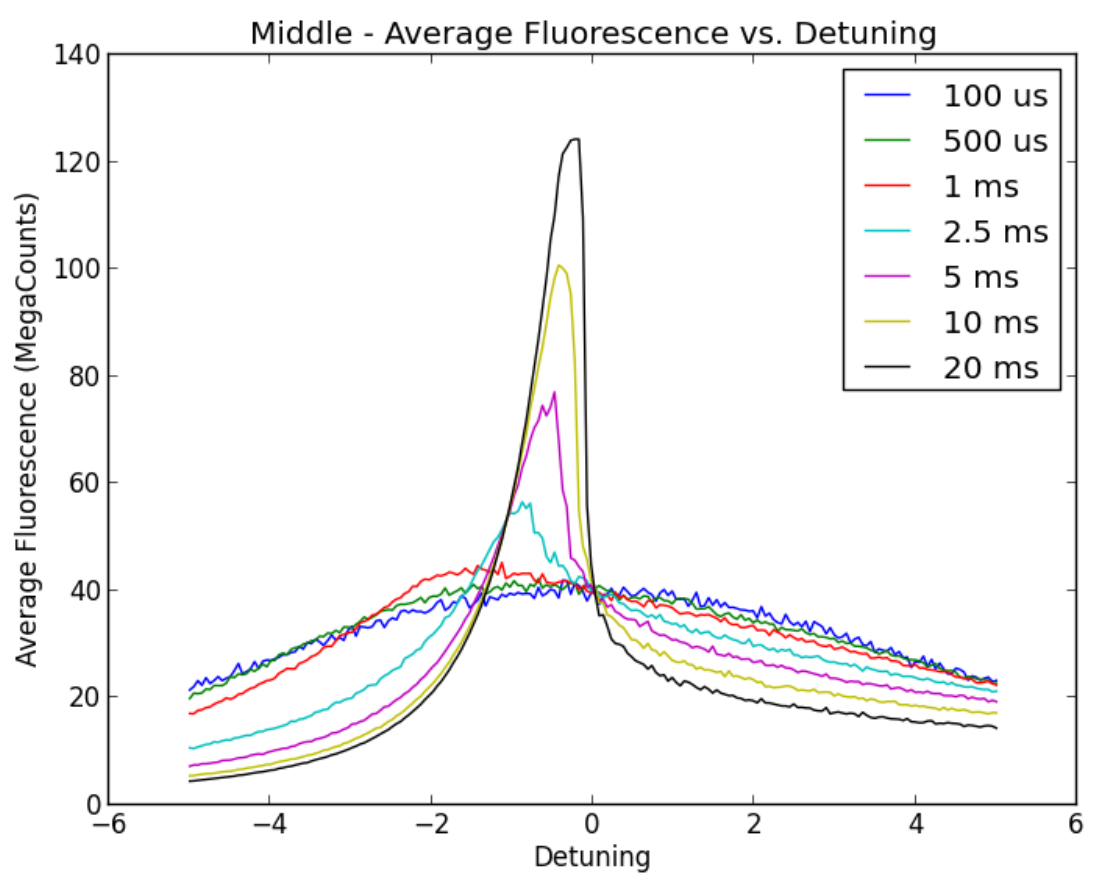


Figure 18: Spectra of the "middle" crystal taken with different readout times.

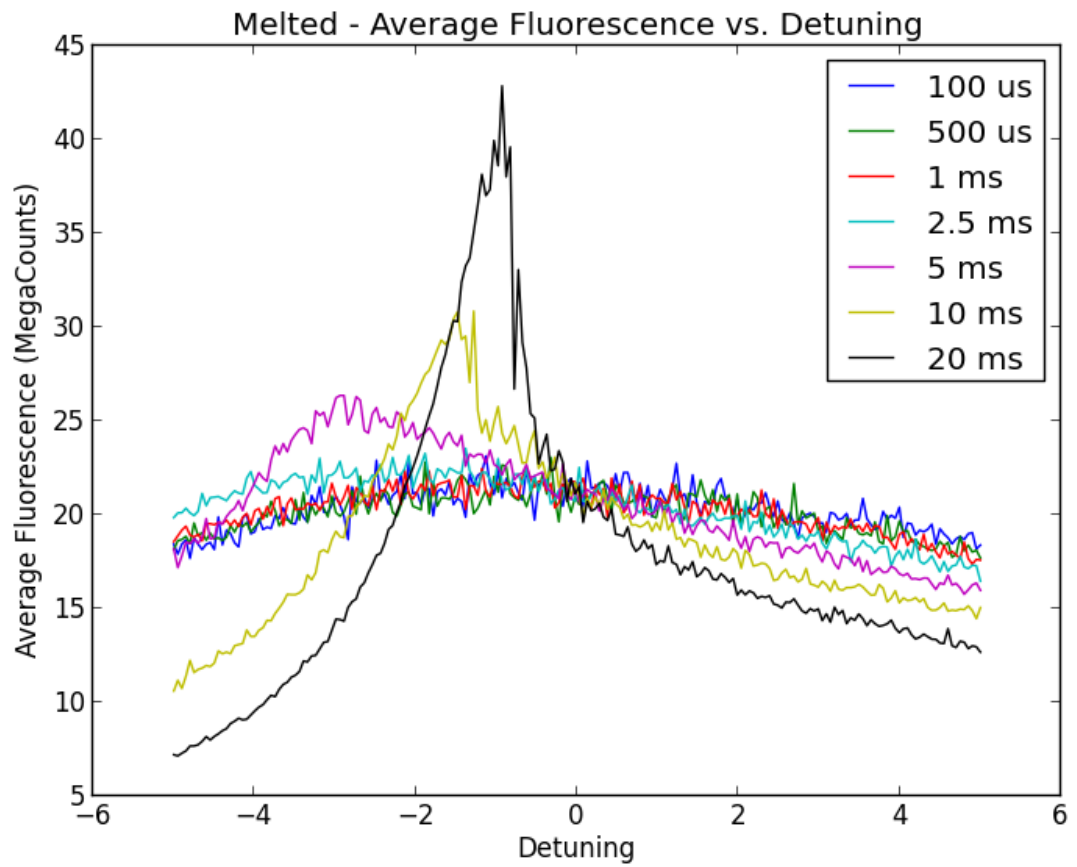


Figure 19: Spectra of the "melted" crystal taken with different readout times.

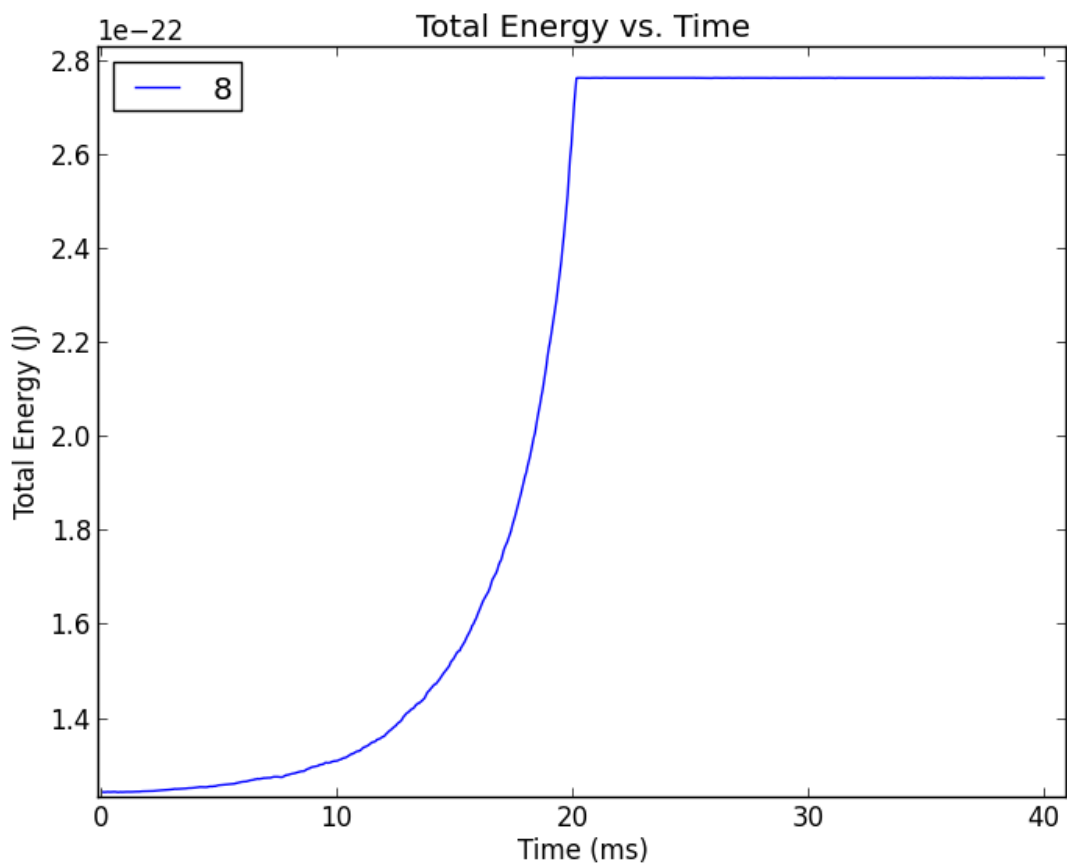


Figure 20: Total energy curve using the pseudopotential.

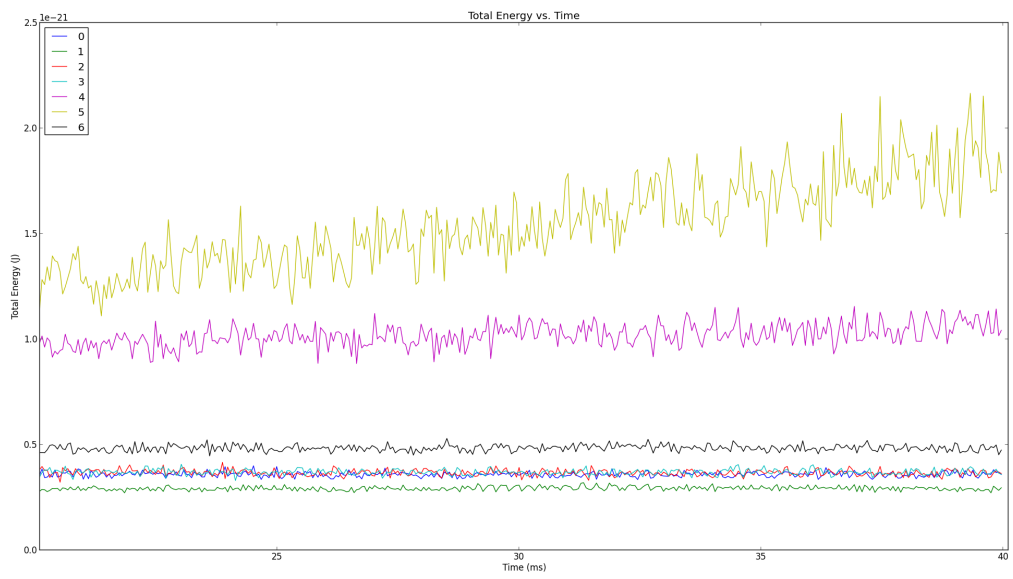


Figure 21: Total energy curve measuring RF heating.

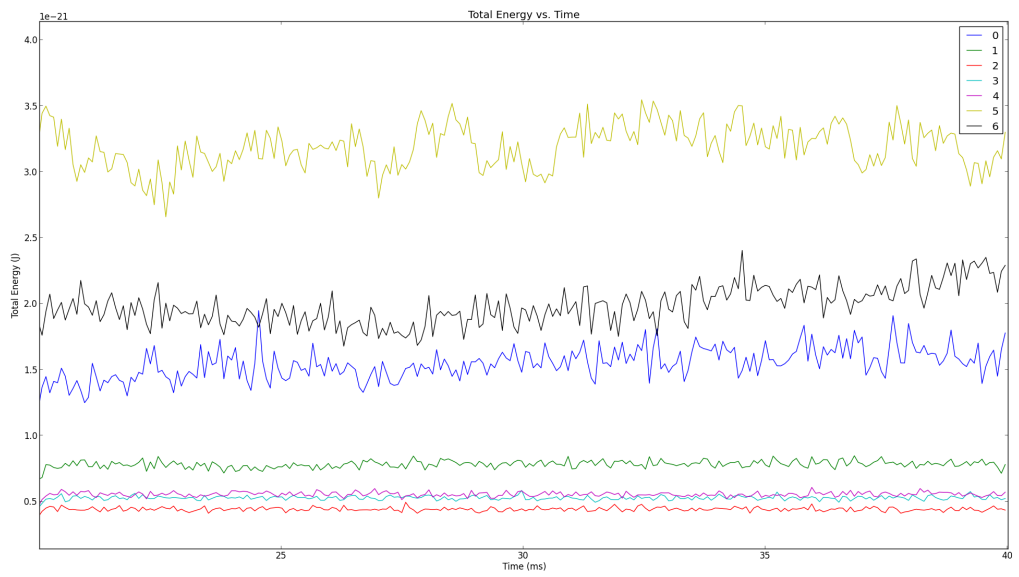


Figure 22: Total energy curve measuring RF heating with a constant electric field.

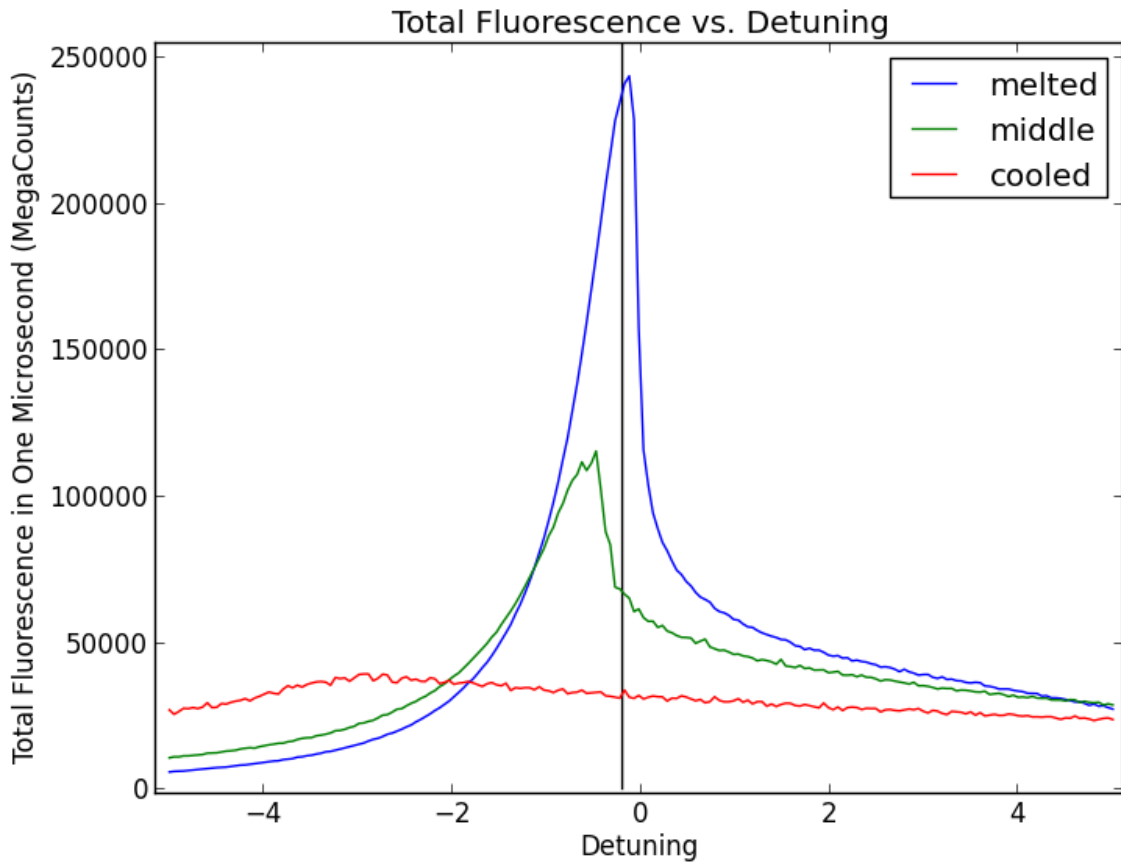


Figure 23: Choosing a readout frequency.

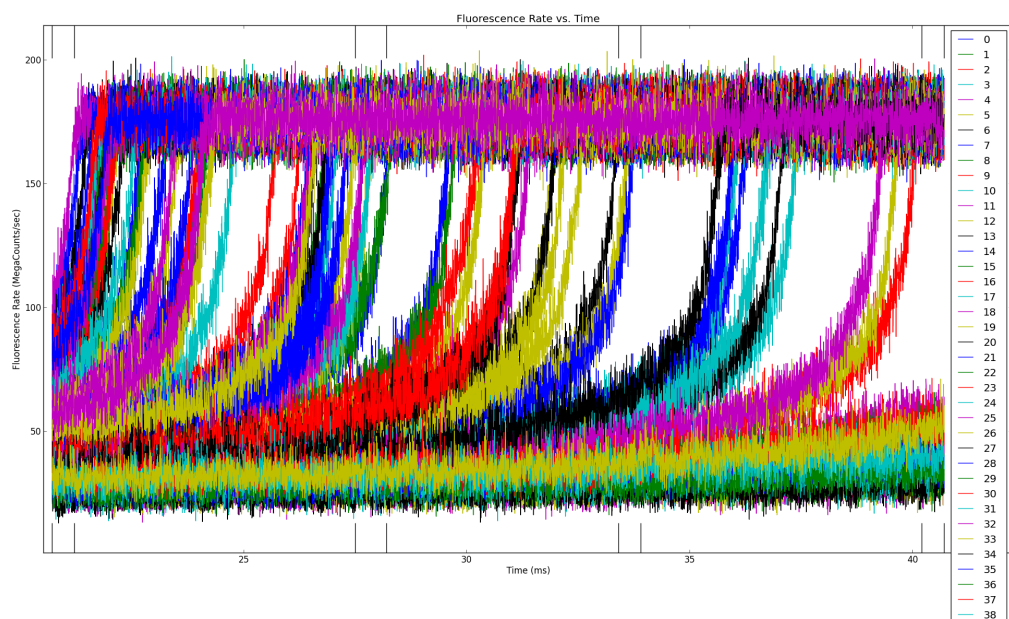


Figure 24: Fluorescence curves after heating - 20 ms readout.

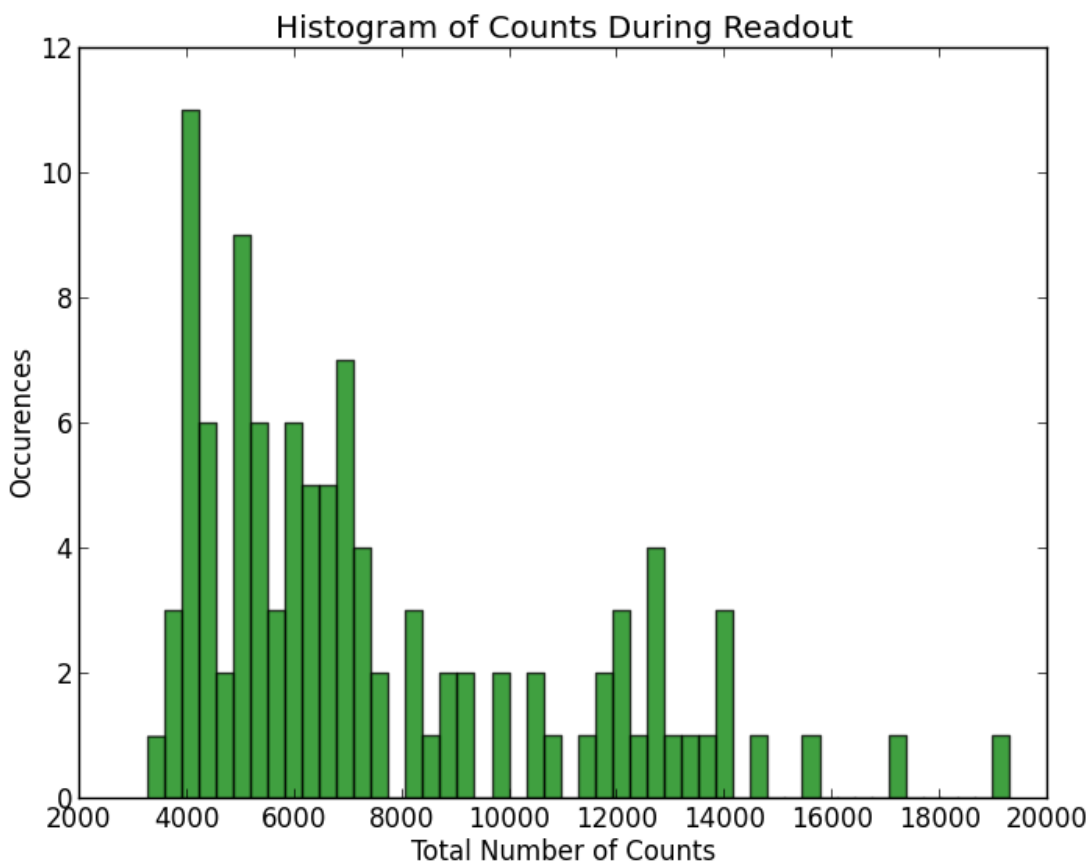


Figure 25: Total fluorescence recorded for first segment.

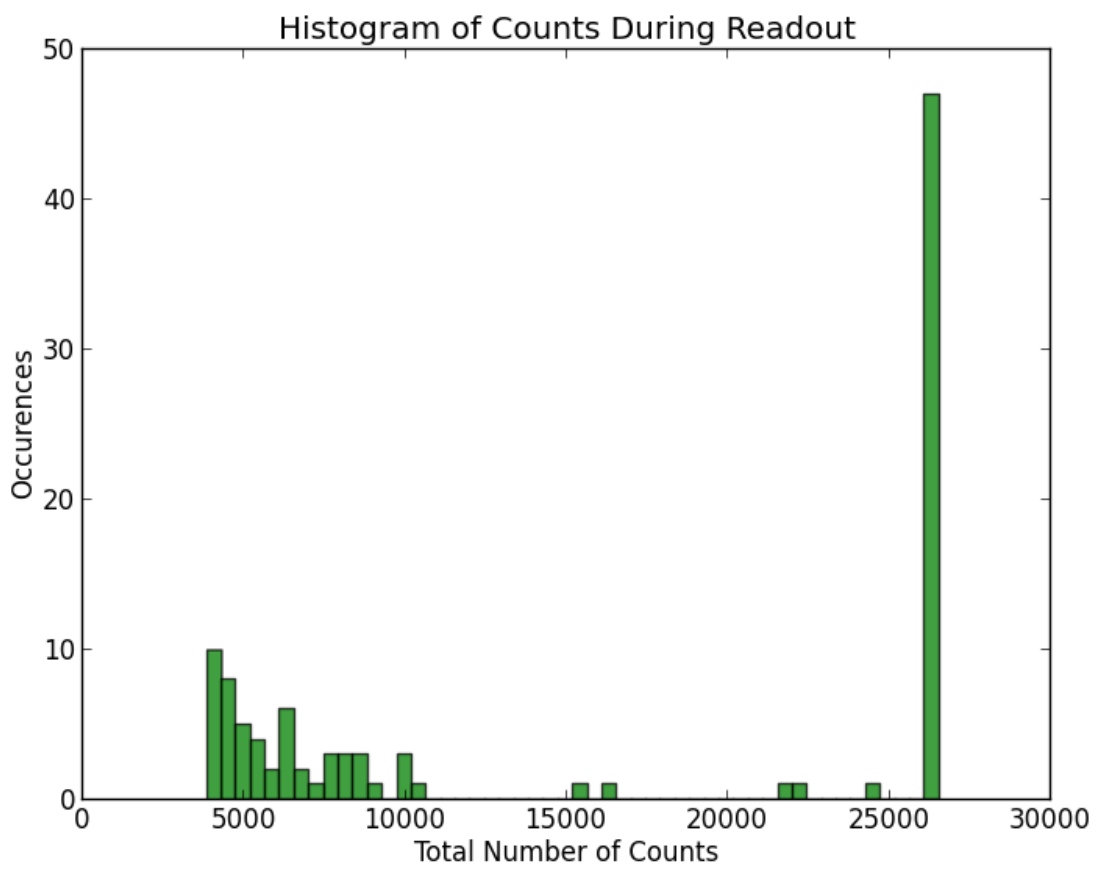


Figure 26: Total fluorescence recorded for second segment.

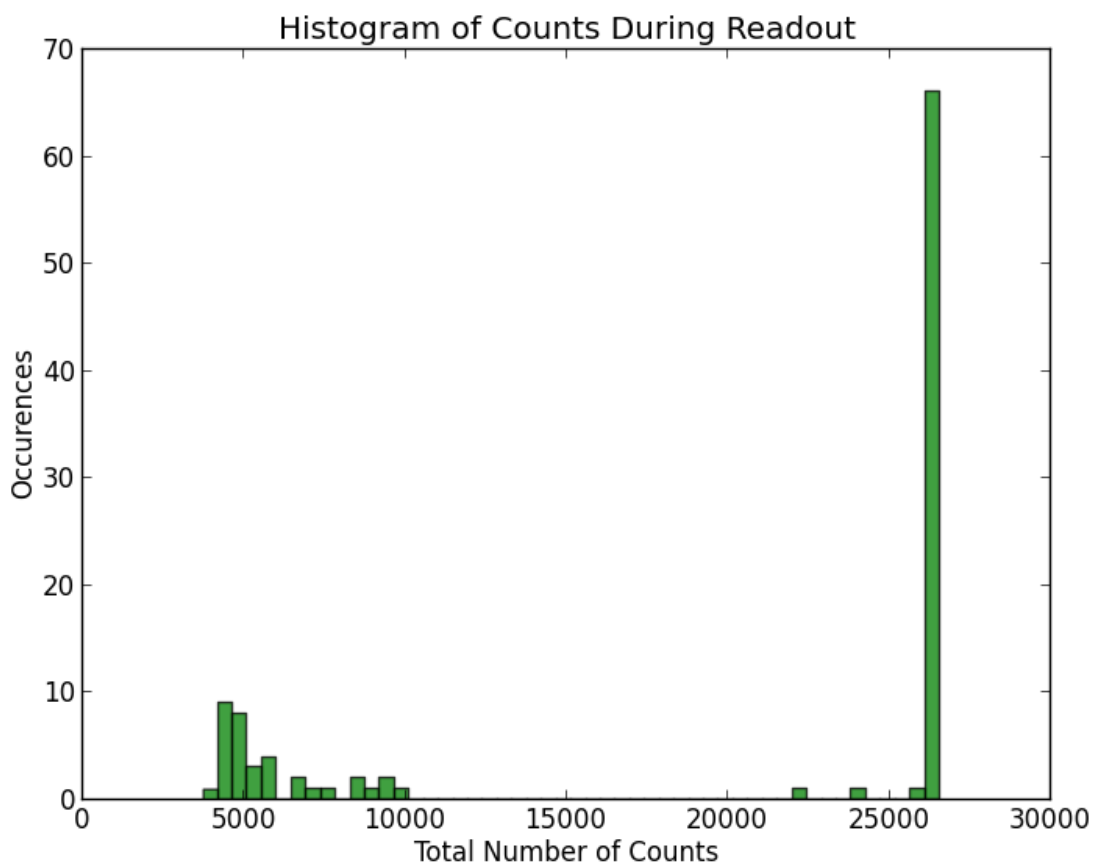


Figure 27: Total fluorescence recorded for third segment.

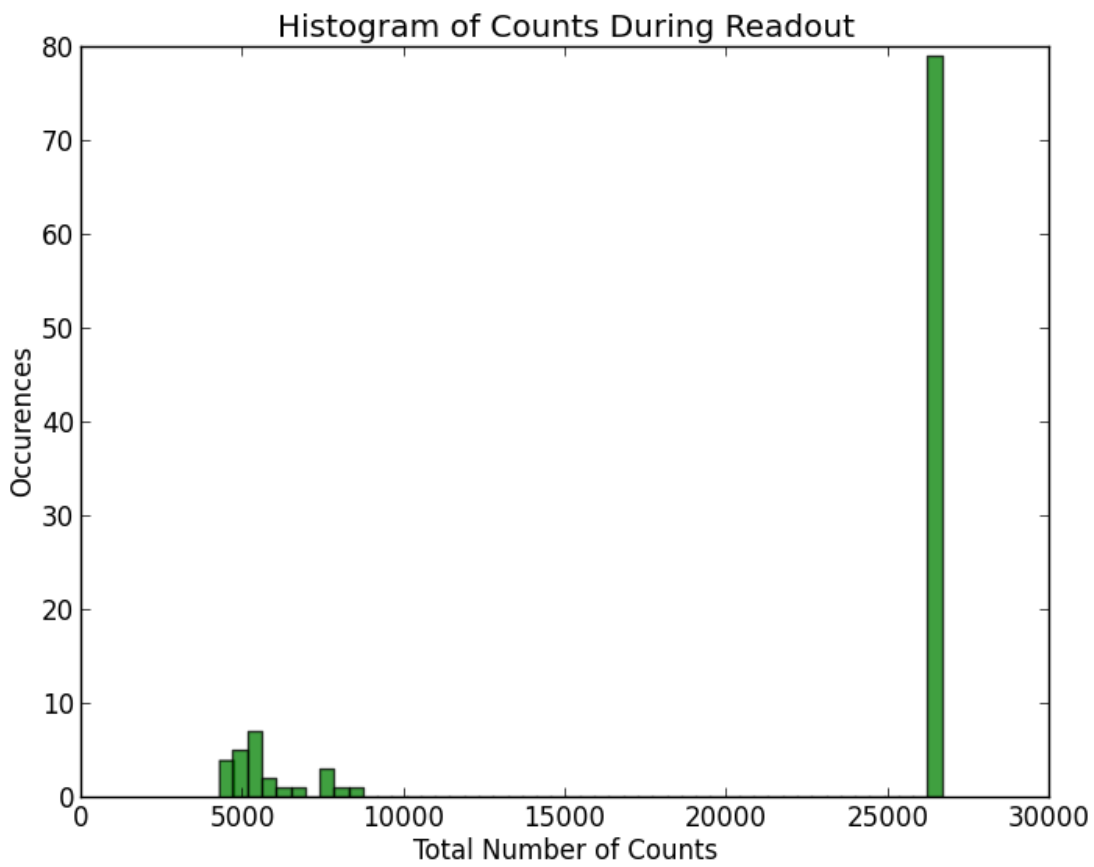


Figure 28: Total fluorescence recorded for final segment.

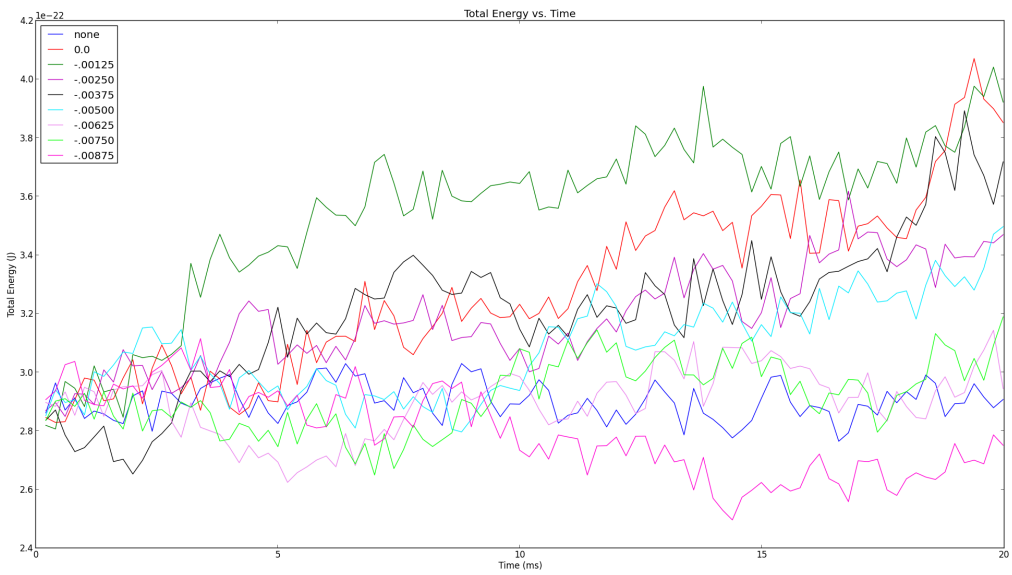


Figure 29: Total energy curves for different readout frequencies - "cooled".

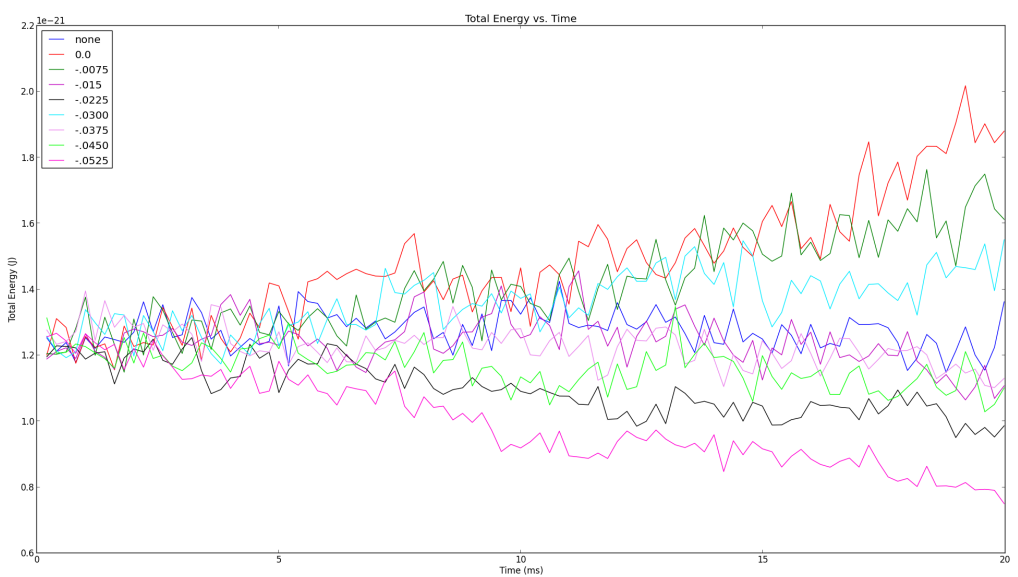


Figure 30: Total energy curves for different readout frequencies - "middle".

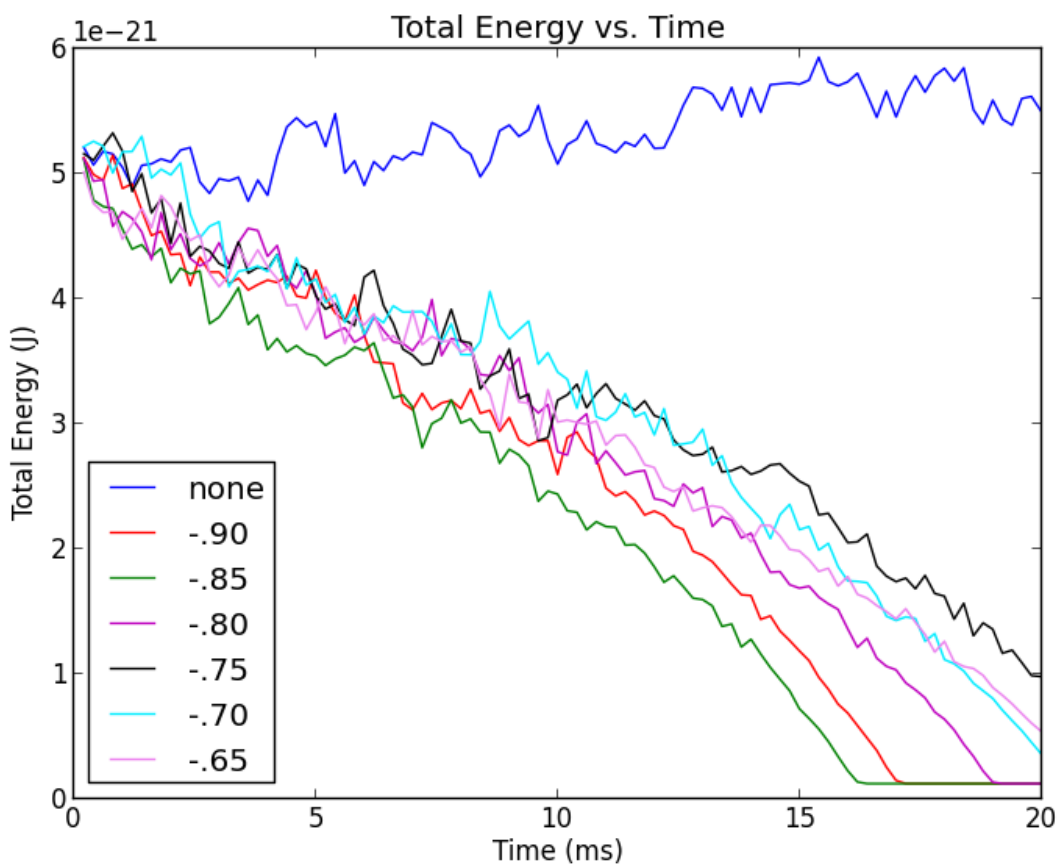


Figure 31: Total energy curves for different readout frequencies - "melted".